Study of the Aerodynamic Sampling Effects of a Holographic Cloud Droplet Instrument

Harri Juttula
Unit of Measurement Technology
University of Oulu
Kajaani, Finland
harri.juttula@oulu.fi

Ville Kaikkonen
Unit of Measurement Technology
University of Oulu
Kajaani, Finland
ville.kaikkonen@oulu.fi

Anssi Mäkynen
Optoelectronics and Measurement Techniques
University of Oulu
Oulu, Finland
anssi.makynen@oulu.fi

***Abstract*—Computational fluid dynamics and particle tracing simulations are presented for a cloud droplet sensor. Airspeeds and streamlines around the sensor are calculated at several wind speeds and their effect on the droplet sampling are examined. Particle tracing is used to study the effect of different wind speeds and droplet sizes on the sampling of the cloud droplets. Simulated droplet concentrations are confirmed by comparing them with measured wind tunnel data. Results demonstrate clear sampling effects that are functions of both wind speed and droplet size. Optimal compromise between maximal measurement volume and sampling effects is found and a simple approximation for sensor's sampling bias is presented. The results show that CFD simulations can give valuable information about the sampling of droplets in an ideal environment with known droplet concentrations. Even in a wind tunnel, the true test conditions are often impossible to accurately determine. Thus by simulating the sampling effects in different conditions, the sensor can be calibrated for a wide range of naturally occurring cloud conditions.**

***Index Terms*—isokinetic flow, CFD simulation, particle tracing, cloud droplet spectrometer, icing, wind energy**

I. Introduction

Wind turbines are affected by accumulation of ice in the turbine blades in cold climates and in high altitudes where freezing conditions are common. Accumulation of ice changes the aerodynamical properties of the blades [1] and lead to production losses and additional maintenance [2], [3]. Cloud icing is a complex process that depends on temperature, wind speed, water content and droplet size distribution of atmosphere and aerodynamic properties of the structure under icing conditions.

The most important parameters when predicting ice formation are liquid water content (LWC) of air and the median volume diameter (MVD) of the droplets and therefore it is of utmost importance that they are measured as accurately as possible. Currently there is no standardized nor traceable way to measure LWC and MVD in low-level clouds [4] even though there exists some commercial and research instruments for their measurement [5]–[8]. The sensor should be able to reliably detect and measure cloud droplets whose size varies from 5 µm to 200 µm in diameter. This is not a straightforward task due to their low concentration and the aerodynamic effects caused by the incorrect probe design. Droplet concentrations and their size distributions may be affected by changes in wind direction and speed or by turbulent airflow inside the measurement volume. The probe may shatter or deflect droplets into or out from the measurement volume [9].

Instrument design affects the droplet concentration if the inlet speed v of the probe is different than the ambient wind speed v_0 [10]. Computational fluid dynamics (CFD) can be used to study if the isokinetic sampling condition ($v_0/v = 1$) is met. Even though isokinetic (or near isokinetic) sampling is crucial for accurate LWC and MVD measurements, it is not uncommon, however, to see it neglected. In non-isokinetic sampling conditions, however, a complex correction algorithm or long test runs are needed to calibrate the instrument for all possible droplet size and wind speed combinations.

In this work, we have used computational fluid dynamics simulation to study the isokinetic sampling condition of a cloud droplet instrument. Additionally we have used the results of CFD simulation as input to particle tracing simulations to study sampling effects as function of both wind speed and droplet size. We have compared the simulation results against real sensor data from controlled wind tunnel tests. While results are valid only for this particular instrument design they demonstrate the need for modeling the aerodynamical effects of any sensor on the airflow and droplets with different diameters.

II. Cloud droplet sensor

Mechanically the droplet sensor consists of sensor body, tail and two identical sensor arms with sharp conical air guides. 3D rendered CAD model of the sensor is shown in Fig. 1. First sensor arm contains laser illumination source while the second arm contains an image sensor. The inner surfaces of the sensor contain multiple heating elements for anti-icing of the outer surface of the sensor. Sensor body houses the control unit and external communications. The sensor is connected to a pole with a freely rotating axle which allows the tail to orient the sensor arms in a direction of the wind.

The laser and the image sensor form a holographic imaging system that can detect cloud droplets from the air flow-

This work was supported in part by European Regional Development Fund (ERDF) under European Territorial Cooperation (ETC) program Interreg V A Nord through Grant NYPS 20202472 and in part by Regional Council of Lapland through Grant 126/00.01.05.24.02/2019.

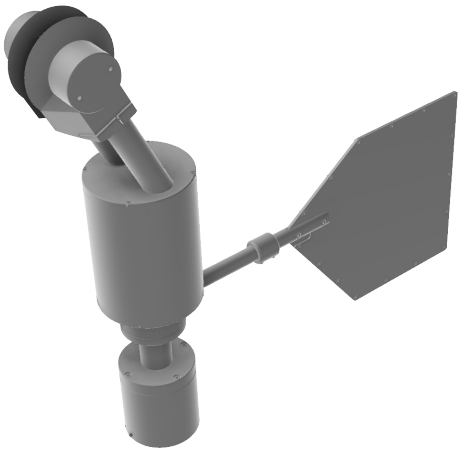

Fig. 1. 3D rendering of the cloud droplet sensor. Measurement volume is located at the center of two symmetrical arms at the top of the sensor body. Airflow is directed between the arms by conical knife-edge air guides.

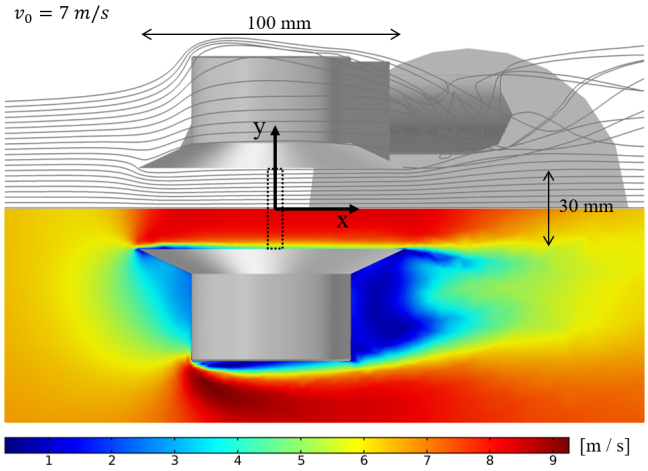

Fig. 2. Top-down view of the 3D simulation model of the droplet sensor with initial wind speed of 7 m/s. Upper half of the figure illustrates the airflow around the sensor while bottom half shows the magnitude of the air velocity. Dashed rectangle between sensor arms shows the measurement volume. Coordinate axes are placed in the global origin.

ing through the sampling volume between the arms. The instrument uses pulsed coherent illumination to capture the interference patterns of the droplets within the sample volume. Details of the holographic measurement principle and the cloud droplet sensor are described in [11], [12]. One of the advantages of the holographic imaging system is that it provides both size and position information of individual droplets. Due to this property, the sample volume shape can be adjusted to provide a data set which best describes free air conditions. It is possible to ignore parts of the measurement volume in post processing of raw data if the sampled droplet concentration is distorted due to aerodynamical effects, for example.

Overall prototype design shown in Fig. 1 is a result of an ad hoc process to design a simple rotating sensor that can withstand strong winds and icing conditions. Sharp knife-edge air guides were added to the design for better airflow and protection from shattered droplets. CFD simulations were used during prototyping to adjust arm lengths and angles to minimize changes to the wind speed and direction entering the imaging volume between the arms. The separation of the air guides is 30 mm and their diameter is 100 mm.

III. Flow simulations and droplet tracing

First let us define the global coordinate system we used in the simulations and in this paper systematically. Origin of the coordinate system is located at the center of the measurement volume illustrated by the dashed rectangle between sensor arms in Fig. 2. Positive x-axis is in a direction of the wind and positive z-direction is upwards. Y-axis is perpendicular to the sensor arm walls which are located at -15 mm and 15 mm distances from the origin.

COMSOL Multiphysics 5.4 was used to perform CFD simulations and droplet tracing calculations. CFD simulations and droplet tracing were done separately so that COMSOL's particle tracing module used the air speed and pressure solution of CFD simulation to solve the forces acting on droplets. Simulated air volume extended 0.6 meters upstream and 1.8 meters downstream from the measurement volume between the arms. Air volume was divided into approximately 800 000 tetrahedral volume elements. An adaptive meshing algorithm was used so that volume elements near the sensor were smaller than far from the sensor. No slip condition was used on the sensor walls. Additionally special thin boundary layer elements were used close to the sensor surface. Stationary solutions for airflows were solved using Reynolds-averaged Navier-Stokes equations and κ-ϵ turbulent flow model [13]. In preliminary simulations the outer boundaries of the air volume were observed to be sufficiently far away from the sensor model so that air velocity at the edges of the system could be considered unaffected by the sensor. Several wind speeds were simulated between 5 to 20 m/s.

For each wind speed particle tracing module was used to trace 100 000 water droplets through the sensor's measurement arms. Initial velocity of the droplets were set to match the wind speed at release. Drag forces due to changes in air speed and pressure were taken into account while gravity was ignored. Six droplet diameters between 5 to 200 µm were simulated. For each release of droplets position and velocity of the droplets passing through yz-plane at $x = 0$ between the sensor arms were recorded for analysis.

Results of the CFD simulations are illustrated in Fig. 2 and Fig. 3. From the simulations it is clear that the flow is not isokinetic ($v/v_0 \neq 1$) and some amount of sampling of droplets may be expected since the streamlines entering the measurement volume are slightly curved and the inlet speed is higher than ambient wind speed. In x-direction wind speed decreases before the sensor arms and then accelerates

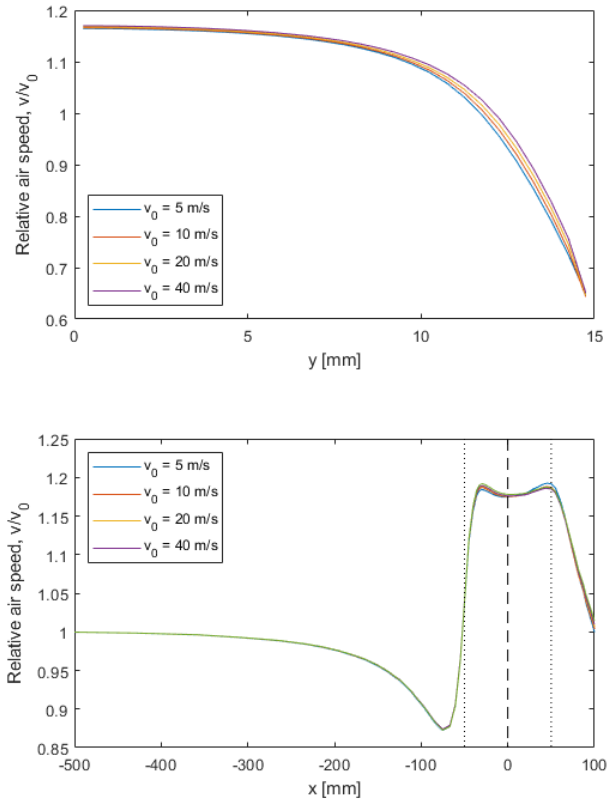

Fig. 3. Relative wind speed profiles at different ambient wind speeds between the sensor arms inside the measurement volume (up) and directly upstream from the measurement volume (down). Dashed line in lower figure shows the location of measurement volume and dotted lines show the extent of the knife edge air guide. It can be seen that relative wind speed profiles are nearly identical at all simulated ambient wind speeds.

to approximately $1.18v_0$ when airflow enters the gap between the arms. In z-direction there are no significant changes in wind speed or direction. Knife-edge air guides slice the air volumes before they are circumvented around the sensor and sample volume is not strongly affected. Near the sensor walls, wind speeds decrease rapidly and a laminar speed profile starts to develop. Fig. 3 shows the average air speed in the sample volume and in upstream at all simulated wind speeds. It can be observed that the velocity profiles have not fully developed into laminar profiles and that the relative profiles are practically identical at all wind speeds.

IV. Wind tunnel tests

To validate the simulations measurements were done with the instrument in icing wind tunnel environment. In the experiments, the sensor was aligned in the direction of the wind while various combinations of wind speed, temperature and water droplet concentrations were tested. One test period provided comparable droplet concentration data against our simulations. The wind tunnel was set to have wind speed v_0 = 7 m/s and temperature $T = -5$ C. Small water droplets were injected into the airflow to create artificial icing condition simulating cloud icing conditions. The instrument accumulated droplet position and size data for a 24-minute period with a 1.5 cm^3/s sampling rate.

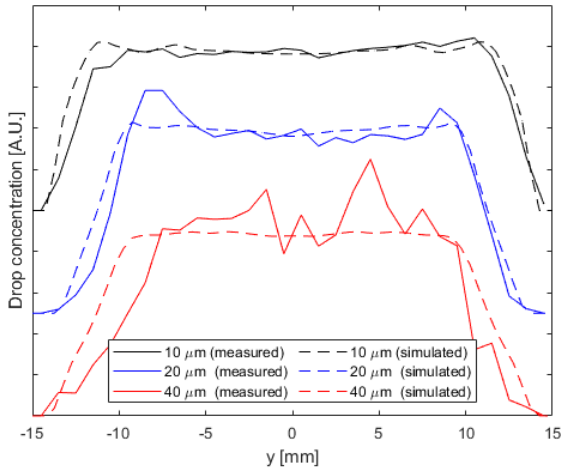

Fig. 4. Comparison of simulated and measured droplet concentration data for three drop diameters. Wind speed was set to 7 m/s in both simulations and measurements. Measurements were done in a wind tunnel. Each concentration profile is normalized by its own sum over the whole y-range and offset is added to 10 μm and 20 μm cases for better visualization. Both simulated and measured droplet concentrations are zero at the sensor walls ($|y| = 15$ mm).

Detected droplet distributions from the wind tunnel test along the y-axis of the measurement volume are shown for 10, 20 and 40 μm droplets in Fig. 4. Measured droplet concentrations are the averages of all droplets within certain upper and lower diameter limits around the nominal values. Limits were ±2 μm, ±3 μm and ±10 μm respectively. Larger averaging limits for the 40 μm droplets are due to a low total number of large droplets since the majority of the droplets in the wind tunnel were in range between 5-20 μm. Total LWC of up to 0.3 g/cm^3 were used in the measurements. The ground truth of the size distribution of the droplets in the wind tunnel was unknown and no other droplet size measurement instruments were available.

Measured and simulated droplet concentrations are in good agreement. Additionally, speed of the droplets were analyzed from consecutive frames and found to be in good agreement with the velocities predicted by the simulations. These observations indicate that our CFD and particle tracing models are valid and can be used to further improve the design in order to achieve isokinetic sampling.

V. Results

Summary of the droplet concentrations relative to ambient concentration at four simulated wind speeds are shown in Fig. 5. Concentration profiles are also scaled by the average droplet speed at each y-coordinate since the detection probability of the pulsed measurement of the real sensor is proportional to the droplet speed. The concentration profiles of Fig. 5 show that

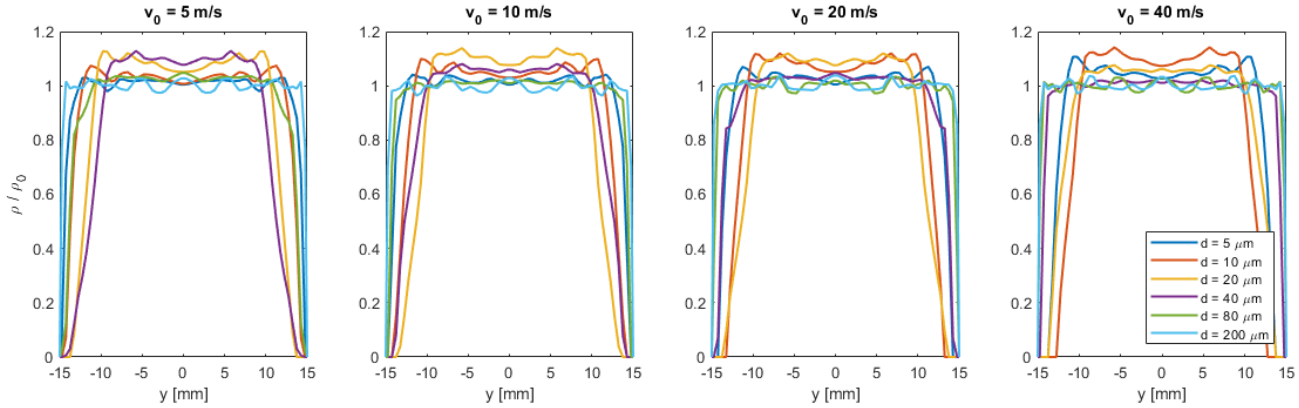

Fig. 5. Simulated relative droplet concentration profiles in the measurement volume between the arms for each droplet size at different wind speeds. Concentrations are approximately constant between -10 to 10 mm and they are within 10% of the free air droplet concentration. Near the sensor wall droplet concentration approaches zero rapidly.

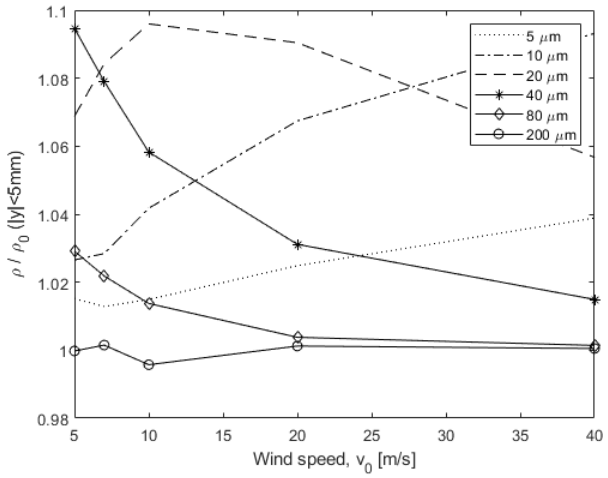

Fig. 6. Relative droplet concentration at the center of measurement volume. Although simulations predict slight overestimation of concentration for all but the largest droplets, they all remain within 10% from the undisturbed free-air concentration ρ_0, which can be considered as a good result for an ad hoc instrument design.

the most massive droplets are nearly unaffected but smaller droplets are directed towards the center. Interestingly, it is not necessarily the smallest 5 µm droplets that exhibit the largest sampling effect as one would intuitively expect. For example, the most overestimated case at $v_0 = 5$ m/s wind speed with approximately 10% increase are the 40 µm droplets while at $v_0 = 40$ m/s the most overestimated droplet size is 10 µm with 10% increase. Overall all droplets below 200 µm are slightly directed towards the center of measurement volume from the sensor walls but the increase in concentration never exceeds 10% of the reference level and the profiles are nearly constant between -10 mm $< y <$ 10 mm.

Average cloud droplet concentrations for each simulated droplet diameter flowing through the center ($|y| < 5$ mm) of the measurement volume at different wind speeds are shown in Fig 6. Concentrations are shown relative to the free air

TABLE I
AVERAGE DIFFERENCE TO FREE AIR CONCENTRATION WITH DIFFERENT SAMPLE VOLUME LIMITS BASED ON DROPLET TRACING SIMULATIONS.

Droplet diameter [µm]	**Difference to ρ_0**		
	Sample volume range		
	full range	**$\|y\| < 10$ mm**	**$\|y\| < 5$ mm**
5	-6.1%	+2.5%	+2.1%
10	-10.9%	+6.3%	+5.1%
20	-15.4%	+8.6%	+7.9%
40	-11.7%	+5.2%	+5.6%
80	-4.0%	+1.3%	+1.4%
200	-0.6%	+0.1%	+0.0%

concentration of droplets ρ_0 at their release. It can be seen that largest ($d = 200$ µm) droplets are not affected by airflow around the instrument while all other droplet sizes experience sampling effects. It is interesting to note that wind speed has opposite sampling effect on small ($5 - 10$ µm) and large ($40 - 80$ µm) droplets while 20 µm droplets seem to be a border case between the two. Reason for this behaviour is probably the combination of the gentle S-shaped airflow trajectory and differences in droplet momentum.

Average differences with respect to the free air concentration for the different sample volume ranges are listed in Table I. Values are calculated as the averages over all simulated wind speeds. If the full range between the sensor arms were used, the sensor would underestimate the droplet concentration by up to -15.4% on average but for some wind speed and droplet diameter combinations the differences can be nearly -20%. If the ability of the holographic measurement to reject droplets in certain y-ranges is utilized by limiting the sample volume to $|y| < 10$ mm, the absolute values of the differences are approximately halved. Based on the relative concentration profiles in Fig. 5 and the average deviations in Table I a practical compromise for minimal sampling effects and maximal measurement volume for the droplet sensor is to reject droplets that are within five millimeter distance from the sensor walls. We found out that by limiting the measurement volume to $|y| < 10$ mm a very good approximation for the

relative droplet concentration for this sensor design is:

$$\frac{\rho(v_0, d)}{\rho_0} = 0.0999 \exp\left(-\frac{(\ln d - \mu(v_0))^2}{2\sigma^2}\right) + 1 \quad (1)$$

Here d is the droplet diameter and v_0 is ambient wind speed. Parameters $\mu(v_0)$ and σ are fitting parameters that can be expressed as $\sigma = 0.6626$ and $\mu(v_0) = -0.48 \ln v_0 + 4.099$. Approximation (1) deviates less than one percent from the simulated relative concentration values for all wind speed v_0 and droplet diameter d combinations used in the simulations. If up to 10% overestimation of the droplet concentration is not acceptable for this sensor design (1) can be used to calibrate measurement values to better match the ambient droplet concentration. Calibration may be more important at lower wind speeds if the LWC and MVD values of the clouds are determined since larger than 20 μm droplets typically dominate these values.

VI. Conclusions

Accurate measurement of cloud droplet sizes and their distributions are challenging. Any sensor structure that measures droplets from an airflow need to consider the aerodynamical sampling effects caused by its own structure. Deviations from the isokinetic sampling conditions can be minimized during the design process by using CFD simulations to optimize the sensor designs.

In this work, we used CFD simulations and particle tracing capabilities of COMSOL Multiphysics software to evaluate how the cloud droplet sensor shown in Fig. 1 affects both the airflow and the droplets that are carried by wind. CFD simulations were performed at several wind speeds that cover the typical wind speeds the sensor is expected to encounter in its install locations. Particle tracing also considered several droplet sizes covering the lower and upper performance limits of the sensor while emphasizing small droplets that are more common in low atmospheric icing conditions. Simulation results were in agreement with real measurement data from the wind tunnel tests. Results show that the current instrument design is not optimal but has sampling effects causing minor errors. According to results, the sensor can measure droplet concentration for all tested wind speeds and droplet sizes with up to +10% overestimation when droplets whose distance from the probe walls is larger than 5 mm are taken into account. Relatively simple approximation of the overestimation as function of wind speed and droplet size was formulated for this sensor design if more accurate concentration measurements are needed.

References

[1] J. Y. Jin, M. S. Virk, "Study of ice accretion and icing effects on aerodynamic characteristics of DU96 wind turbine blade profile," Cold Reg. Sci. Technol., vol. 160, pp. 119–127, 2019.

[2] M. C. Homola, M. S. Virk, P. J. Nicklasson, P. A. Sundsbo, "Performance losses due to ice accretion for a 5 MW wind turbine," Wind Energ. vol. 15, no. 3, pp. 379–389, 2012.

[3] V. Turkia, S. Huttunen, T. Wallenius, "Method for estimating wind turbine production losses due to icing," Espoo: VTT Technical Research Centre of Finland, VTT technology, no. 114, 2013.

[4] A. Krenn et al., "Available technologies for wind energy in cold climates," International Energy Agency Wind Task 19, 2016.

[5] D. Baumgardner et al, "Airborne instruments to measure atmospheric aerosol particles, clouds and radiation: A cook's tour of mature and emerging technology," Atmos. Res., vol. 102, pp. 10–29, 2011.

[6] S. Rydblom, B. Thörnberg, "Liquid Water Content and Droplet Sizing Shadowgraph Measuring System for Wind Turbine Icing Detection," IEEE Sens. J., vol. 16, no. 8, 2016.

[7] J. Henneberger, J. P. Fugal, O. Stetzer, U. Lohmann, "HOLIMO II: a digital holographic instrument for ground-based in situ observations of microphysical properties of mixed-phase clouds," Atmos. Meas. Tech., vol. 6, pp. 2975–2987, 2013.

[8] S. Lance, C. A. Brock, D. Rogers, J. A. Gordon, "Water droplet calibration of the Cloud Droplet Probe (CDP) and in-flight performance in liquid, ice and mixed-phase clouds during ARCPAC," Atmos. Meas. Tech., vol. 3, pp. 1683–1706, 2010.

[9] A. Korolev, E. Emery, K. Creelman, "Modification and Tests of Particle Probe Tips to Mitigate Effects of Ice Shattering," J. Atmos. Oceanic Technol., vol. 30, pp. 690–708, 2012.

[10] J. D. Wilcox, "Isokinetic Flow and Sampling," J. Air Pollut. Control Assoc., vol. 5, No. 4, pp. 226–245, 1956.

[11] V. A. Kaikkonen, D. Ekimov, A. J. Mäkynen, "A Holographic In-Line Imaging System for Meteorological Applications," IEEE Transactions on Instrumentation and Measurement, vol. 63, no. 5, 2014.

[12] V. A. Kaikkonen, E. O. Molkoselkä, A. J. Mäkynen, "Droplet size distribution and liquid water content monitoring in icing conditions with the ICEMET sensor," in Proc. Int. Workshop on Atmospheric Icing of Structures, Reykjavik, Iceland, 2019.

[13] D. C. Wilcox, Turbulence Modeling for CFD, 2nd ed., DCW Industries, 1998.